Propagation modeling results for narrow-beam undersea laser communications

Andrew S Fletcher, Nicholas D. Hardy, Scott A. Hamilton

Andrew S Fletcher, Nicholas D. Hardy, Scott A. Hamilton, "Propagation modeling results for narrow-beam undersea laser communications," Proc. SPIE 9739, Free-Space Laser Communication and Atmospheric Propagation XXVIII, 97390I (15 March 2016); doi: 10.1117/12.2222890

SPIE.

Event: SPIE LASE, 2016, San Francisco, California, United States

Propagation Modeling Results for Narrow-beam Undersea Laser Communications

Andrew S. Fletcher, Nicholas D. Hardy, Scott A. Hamilton
MIT Lincoln Laboratory, 244 Wood St., Lexington, MA, USA 02421

ABSTRACT

Communication links through ocean waters are challenging due to undersea propagation physics. Undersea optical communications at blue or green wavelengths can achieve high data rates (megabit- to gigabit-per-second class links) despite the challenging undersea medium. Absorption and scattering in ocean waters attenuate optical signals and distort the waveform through dense multipath. The exponential propagation loss and the temporal spread due to multipath limit the achievable link distance and data rate. In this paper, we describe the Monte Carlo modeling of the undersea scattering and absorption channel. We model photon signal attenuation levels, spatial photon distributions, time of arrival statistics, and angle of arrival statistics for a variety of lasercom scenarios through both clear and turbid water environments. Modeling results inform the design options for an undersea optical communication system, particularly illustrating the advantages of narrow-beam lasers compared to wide beam methods (e.g. LED sources). The modeled pupil plane and focal plane photon arrival distributions enable beam tracking techniques for robust pointing solutions, even in highly scattering harbor waters. Laser communication with collimated beams maximizes the photon transfer through the scattering medium and enables spatial and temporal filters to minimize waveform distortion and background interference.

Keywords: Undersea communication, optical propagation, lasercom, narrow beam, wide beam

1. INTRODUCTION

Wideband wireless communication through ocean waters is an area of renewed interest due in large part to the proliferation of unmanned and autonomous undersea vehicles (UUVs and AUVs). Undersea propagation physics places significant limits on signaling methods for communication. The three principal modalities are radio frequencies in the ultra-low or very-low frequencies (<30 kHz), acoustic frequencies below 100 kHZ, or optical frequencies in the visible spectrum (especially blue and green). Optical communication has long been recognized as the most promising method to achieve high data rates, because its propagating bandwidth is several orders of magnitude greater than RF or acoustic. The ocean medium, however, attenuates light exponentially with propagation distance, which limits the achievable link ranges. Propagation is highly dependent on the water clarity; we can anticipate links of hundreds of meter lengths in clear ocean waters, while the turbid waters of a harbor can limit achievable link distances to less than 10 meters. In spite of the short range, the wide bandwidths from undersea optical communication enable important UUV missions for applications in scientific, military and commercial fields.

Several groups have published demonstrations of optical communications through water, with both laboratory and field demonstrations[1-7]. We can see within these demonstrations two distinct approaches regarding signaling. The vehicle demonstration in the Woods Hole Oceanographic Institution[3] transmitted light over a hemisphere, a practical measure that avoided any precision pointing of either terminal. Many of the cited laboratory demonstrations utilize a narrow, often collimated, beam of light from a laser. A deployed narrow-beam optical communication system requires a robust solution to precision pointing, including initial acquisition and tracking through vehicle maneuvers. PAT (pointing, acquisition, and tracking) systems have been demonstrated for numerous laser communication systems in air and space[8]. Inclusion of a PAT system for undersea optical communications has an implementation cost, but also provides benefits in terms of achievable link range, communications bandwidth, and terminal size. In this paper, we quantify through Monte Carlo simulation the predicted benefits of narrow-beam laser communication compared to wide-beam methods.

We start by describing our simulation methodology in Sec. 2, which will be used to investigate the underwater channel for optical communication. The end product of our simulations is an analysis of the underwater channel's information capacity; this analysis spans using narrow and wide beam transmitters, water conditions ranging from a turbid harbor to deep, clear ocean, and a varying aperture size and field of view at the receiver. To inform this analysis we first

Free-Space Laser Communication and Atmospheric Propagation XXVIII, edited by
Hamid Hemmati, Don M. Boroson, Proc. of SPIE Vol. 9739, 97390I · © 2016 SPIE
CCC code: 0277-786X/16/$18 · doi: 10.1117/12.2222890

investigate the spatial, angular, and temporal distortions of the beam in Secs. 3, 4, and 5. We then investigate the total energy transferred in the channel as a function of the receiver size in Sec. 6. These results are combined into performance predictions for the various scenarios in Sec.7.

2. PROPAGATION MODEL

Optical propagation through water is in many ways similar to propagation through the atmosphere: light is scattered and absorbed by molecular and atomic interactions, temperature variations cause turbulence, and large suspended particulates cause additional absorption and scattering. Atmospheric communication is primarily affected by turbulence-induced fading and scintillation, and most simulations approximate these effects using a series of phase screens; scattered light generally does not reach the receiver and is treated as loss. In underwater propagation, the large particulate scattering and absorption dominates all other effects and a significant amount of scattered light can reach the receiver. Therefore, most simulations that model underwater propagation use a Monte-Carlo ray tracing approach which models the large particle scattering effects[9-13]. We use this approach in our analysis.

We treat the water as a homogenous medium (or more generally as a composition of layers of homogenous mediums) so that within a body of water the scattering and absorption become Poisson processes, i.e., the likelihood of scattering and absorption events is uniform throughout the volume. This means that the distance X between such events is an exponential random variable with the probability distribution

$$p_X(x) = \alpha e^{-\alpha x}, \quad x \geq 0, \tag{1}$$

with rate parameter α. The exponential distribution is fully characterized by the rate parameter, which for the absorption and scattering processes are the absorption coefficient a (m^{-1}) and scattering coefficient b (m^{-1}). These are often combined to form the extinction coefficient $c = a + b$.

To keep as many photons paths (rays) in the simulator as possible we account for the absorption at the end by weighting the contribution of each photon by how likely it is to have not been absorbed. From Eq. (1) we get a weighting of e^{-aL} for a photon that travels L m during the simulation. The scattering, however, needs to be explicitly modeled and simulated. The strength of scattering in deflection angle θ and azimuthal angle ϕ is contained in the volume scattering function[14] (VSF) $\beta(\theta, \phi)$. The total scattering coefficient b is found from integrating the VSF over all 4π Steradians, i.e.,

$$b = \int_0^{\pi} d\theta \int_0^{2\pi} d\phi \, \beta(\theta, \phi) \sin(\theta). \tag{2}$$

The normalized scattering phase function (SPF) $\tilde{\beta}(\theta, \phi) = \beta(\theta, \phi)/b$ then determines the relative likelihood that a photon scatters in each direction.

To simulate the scattering process we first generate a distance to the next scattering event from an exponential distribution with rate parameter b, and advance the photon along its current trajectory. Next, the scattering deflection and azimuthal angles are generated according to the phase function, and the photon's propagation direction is updated accordingly. This process is repeated until the photon reaches the simulation's boundaries or the simulation ends.

Some of the most widely used ocean characterization measurements were taken by Petzold[15], in which he measured the a and b coefficients and VSF in numerous locations for green light (absorption at 530 nm, scattering at 514 nm). Interestingly, he noted that while the VSF measurements varied in scale (a result of differing b parameters), they all had a similar shape, indicating a similar SPF across water types. Mobley used these data to propose an average ocean water SPF, as well as characteristic a and b parameter values for different water types[9,14]. We will use these water types in our simulations, and they are given in Table 1.

In what follows we use this simulator to characterize the undersea channel for optical communication, presenting results for both a turbid harbor and clear ocean. In the harbor, green light generally propagates best [16], and we are focusing on a system using a 518 nm diode laser; this wavelength is close to that used for Petzold's data, so we will use the a and b values from row 1 of Table 1 in the simulation. Blue light propagates better in clear ocean[16], so we run these

simulation at 470 nm. In deep, clear water extinction coefficients of $c = 0.05$ have been observed at 470 nm[1], but as there is not full characterization data, we will use the scattering albedo b/c for clear ocean at 514 nm with $c = 0.05$.

Table 1: Absorption coefficients (a), scattering coefficients (b) , extinction coefficients (c), and the scattering albedo $w_0 = b/c$ for the water types defined by Mobley[14]. We include a clear ocean case for 470 nm with the extinction value from Pontbriand[1] and the same scattering albedo as the clear ocean case at 514 nm.

Water Type	Wavelength	a ($\mathbf{m^{-1}}$)	b ($\mathbf{m^{-1}}$)	c ($\mathbf{m^{-1}}$)	w_0
Turbid Harbor	514 nm	0.366	1.824	2.190	0.833
Clear Ocean	514 nm	0.114	0.037	0.151	0.247
Clear Ocean	470 nm	0.038	0.012	0.05	0.247

For our simulations we generate scattering angles using the analytic SPF model[11],

$$\tilde{\beta}(\theta,\phi) = \frac{1}{Z}\frac{\exp\left(-(\Theta/\Theta_0)^{1/2}\right)}{4\pi(\Theta/\Theta_0)^{3/2}\Theta_0^2}, \tag{3}$$

where $Z = 1 - \exp(-(2/\Theta_0)^{1/2})$, $\Theta = 2\sin(\theta/2)$ and $\Theta_0 = 2\sin(\theta_0/2)$. This phase function closely fits Mobley's fitted model[9] in the forward angles for $\theta_0 = 0.13$; moreover, its cumulative distribution function is invertible, allowing for efficient generation of scattering angles using inversion sampling.

This model for the SPF allows simulation of a wide range of ocean water types. Yet many laboratory experiment use artificial scattering agents, such as Maalox and Arizona dust, which can have drastically different SPFs. To cross validate our simulator with future laboratory experiments (or in natural waters that do not conform to the standard SPF), we have also developed a method to generate scattering from empirical measurements of the SPF. However, in this paper all simulations use the analytic SPF in Eq. (3).

Our analysis also focuses on two limiting cases for the light's transmission mode. First, we consider a point source that produces uniform-intensity radiation over the forward hemisphere. We will refer to this as the wide beam (WB), and is representative of LEDs or intentionally spoiled laser beams. Alternatively, we consider a collimated laser beam with radial waist w_0, referred to as the narrow beam (NB), which is similar to what is used in atmospheric laser communications. We have chosen to analyze the narrow beam for $w_0 = 0.5$ cm so that the beam is representative of what might be used in a compact terminal that could go on a buoy or unmanned vehicle.

3. SPATIAL ANALYSIS

We first investigate the distortion of the light's transverse spatial distribution as it propagates through the water. We extend our analysis out to 20 extinction lengths, where an extinction length (EL) is c^{-1} m, and corresponds to the average distance travelled before an absorption or scattering event occurs. For our turbid harbor model the extinction length for green light is 0.46 m, while for blue light in clear water it is 20 m. To aid analysis of the spatial distortion of the beam we present the radial profile of the beam at both 10 and 20 EL. These are compared on a normalized decibel scale in Figure 1 for clear water and Figure 2 for harbor water.

We note that in both water types the wide beam's intensity maintains its uniform spatial distribution, but it is much weaker than the narrow beam. In the clear ocean (where absorption dominates scattering) the narrow beam seems to keep its shape—growing slightly in width due to diffraction after several hundred meters—but there is some scattered light outside the main lobe, setting a scattering "floor" of non-direct photons. In the harbor water (where scattering dominates absorption) the narrow beam quickly diffuses, and the central lobe is barely distinguishable from the scattering floor after 20 EL (~10 m) of propagation.

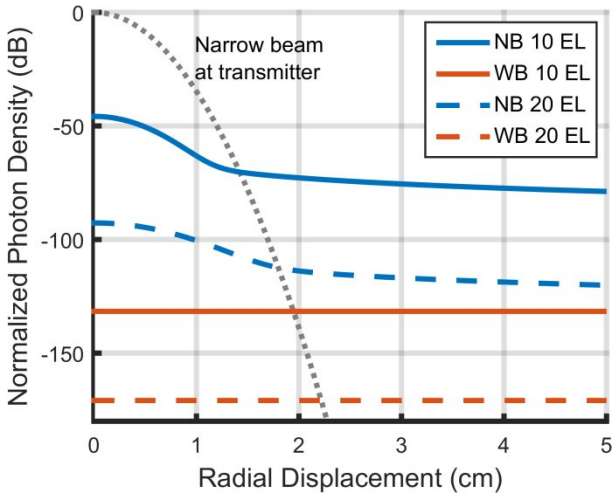

Figure 1: Clear ocean beam profile: radial photon density of narrow beam (NB) and wide beam (WB) at 10 extinction lengths (200 m) and 20 extinction lengths (400 m) in clear ocean water. Plots are in decibels, and normalized to the density of the transmitted narrow beam at the origin.

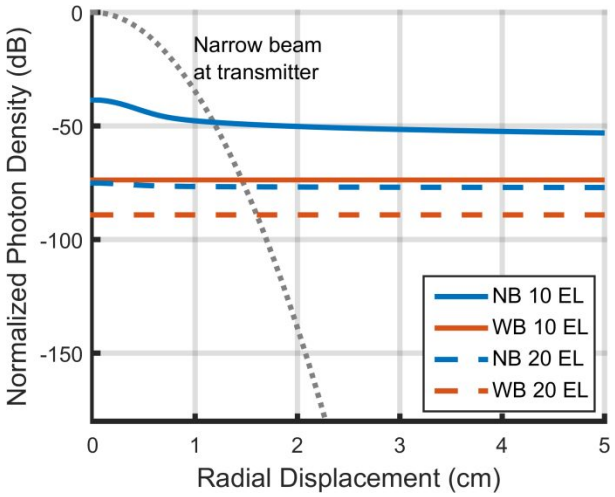

Figure 2: Harbor beam profile: radial photon density of narrow beam (NB) and wide beam (WB) at 10 extinction lengths (4.6 m) and 20 extinction lengths (9.2 m) in turbid harbor water. Plots are in decibels, and normalized to the density of the transmitted narrow beam at the origin.

4. ANGULAR ANALYSIS

In the spatial analysis we saw that in the high-albedo turbid harbor the narrow beam washes out and is not readily distinguishable with a spatial-basis intensity measurement. However, the story is different in the angular basis.

To analyze the angular spectrum of the beam we finish the simulation by passing the photons through a lens with a 1 cm radius and 10 cm focal length (f). We then measure the spatial profile in the focal plane, and convert the radial axis (r) to the angular basis as $\theta = r/f$ (valid approximation for $r \ll f$). We again analyze the propagated light at 10 and 20 EL for both water and source types. In Figure 3 we see that in clear water the angular distribution is mostly unchanged for the narrow beam, with a scattering floor about 40 dB below the peak. For the wide beam the distribution is uniform for angles subtended by the receive aperture ($\theta < L/R$ for propagation distance L and receiver aperture radius R), which are angles that can be reached without scattering; outside these angles we are at the scattering floor.

However, in Figure 4 we see that in the harbor water the narrow beam's main lobe still has about 20 dB of discrimination from the scattering floor. This is in contrast to the spatial distribution where the main lobe disappeared after 20 EL, and indicates that when the beam has washed out spatially it can still be recovered with angular filtering.

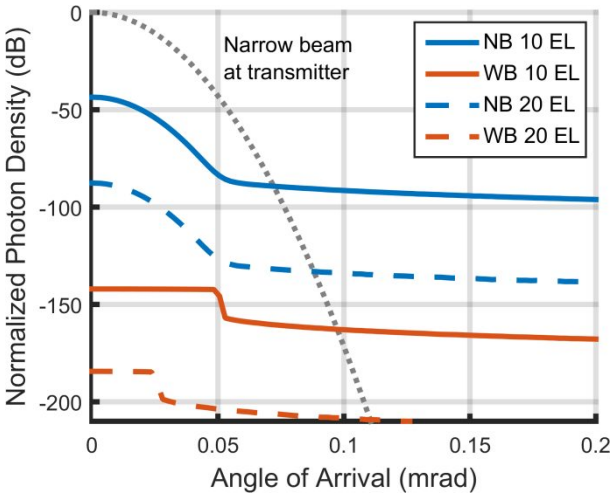

Figure 3: Clear ocean angular beam profile: angular photon density of narrow beam (NB) and wide beam (WB) at 10 extinction lengths (200 m) and 20 extinction lengths (400 m) in clear ocean water. Plots are in decibels, and normalized to the density of the transmitted narrow beam at 0 rad.

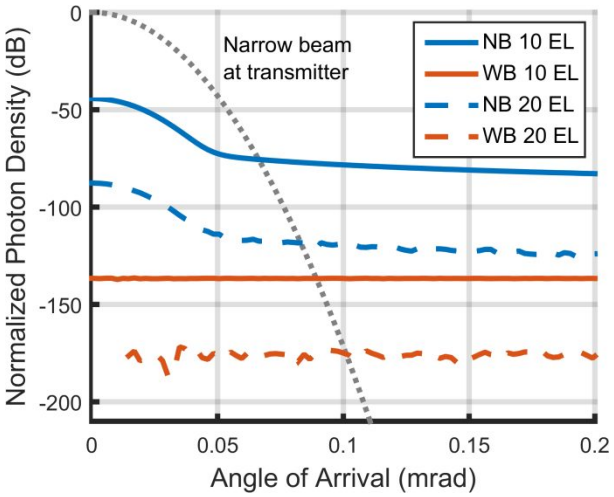

Figure 4: Harbor angular beam profile: angular photon density of narrow beam (NB) and wide beam (WB) at 10 extinction lengths (4.6 m) and 20 extinction lengths (9.2 m) in turbid harbor water. Plots are in decibels, and normalized to the density of the transmitted narrow beam at 0 rad.

To more clearly see this effect, in Figure 5 and Figure 6 we plot the narrow beam's radial photon densities from Figure 1 and Figure 2 together with versions that have a 10 mrad AoA filter. In the clear ocean the AoA filtering causes a suppression of the scattering floor, but the effect is minimal. However, in the turbid harbor the narrow beam's profile is recovered at both distances, and at 20 EL there is still 20 dB of separation between the signal peak and scattering floor.

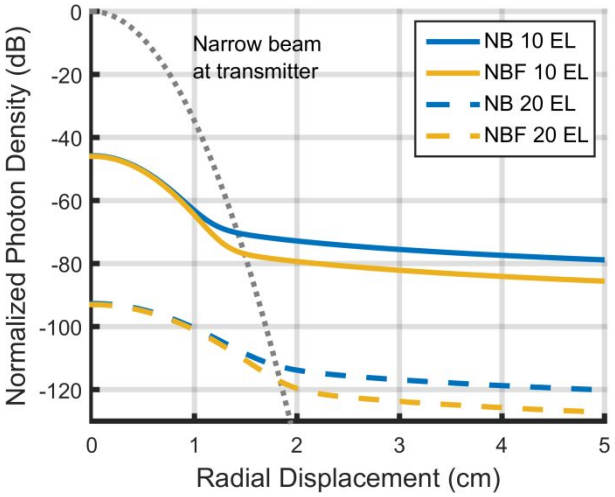

Figure 5: Clear ocean beam profile: narrow beam radial photon density in clear ocean water, both without filtering (NB) and with a 10 mrad filter (NBF). Plots are in decibels, and normalized to the density of the transmitted narrow beam at the origin.

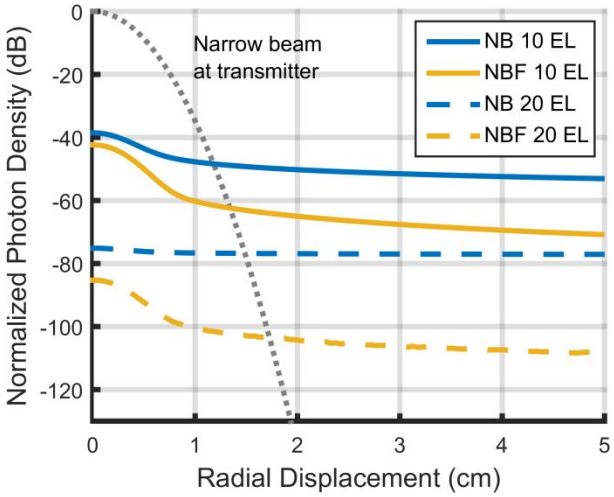

Figure 6: Harbor beam profile: narrow beam radial photon density in turbid harbor water, both without filtering (NB) and with a 10 mrad filter (NBF). Plots are in decibels, and normalized to the density of the transmitted narrow beam at the origin.

5. TEMPORAL ANALYSIS

Next we consider the temporal distortion of the beams. We are primarily concerned with how much light will arrive late enough to cause inter-symbol-interference (ISI) at various modulation rates. We again consider both water types and light sources. However, in the previous section we saw that scattered light is more prominent outside a certain angle-of-arrival (AoA), so we also consider moderate AoA filtering of 10 mrad on the narrow-beam receiver. For the wide-beam receiver, this filtering would require a PAT system, so those results are not included in the graph. We found that in clear water the narrow beam had minimal temporal spreading, and 99% of the light had arrived with less than 10 fsec of delay at both 10 and 20 EL; the angular filtering had a minimal effect. However, for the wide beam, there was significant spreading and over 10% of the light arrived after 10 microseconds at 10 extinction lengths, and after 100 microseconds at 20 extinction lengths. This indicates there will be appreciable ISI at modulation rates of > 10 MHz for the wide beam in clear ocean.

In the harbor, both the wide beam and narrow beam have significant temporal spreading at both 10 and 20 EL. However, the AoA filter removes much of the delayed light in the narrow beam, and less than 1% of the light arrives after a 10 psec. These results indicate that in the harbor the wide beam may have its bandwidth limited by the ISI after 10 EL, while the narrow-beam receiver can filter out much of the scattered light to recover 10-100 GHz of bandwidth out past 20 EL.

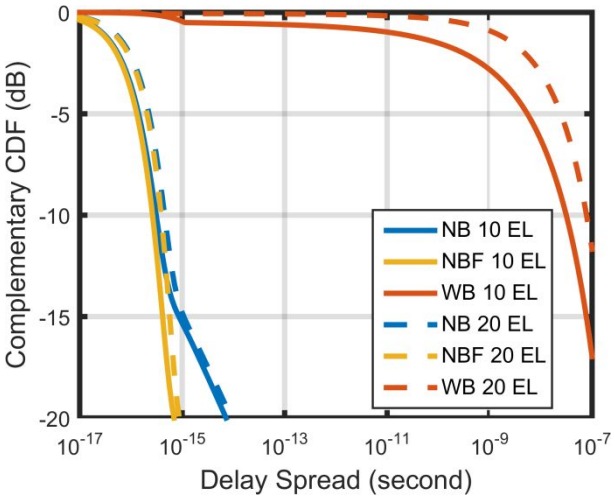

Figure 7: Delay spread of transmitted light in clear ocean water for the narrow beam (NB), 10 mrad filtered narrow beam (NBF) and wide beam (WB).

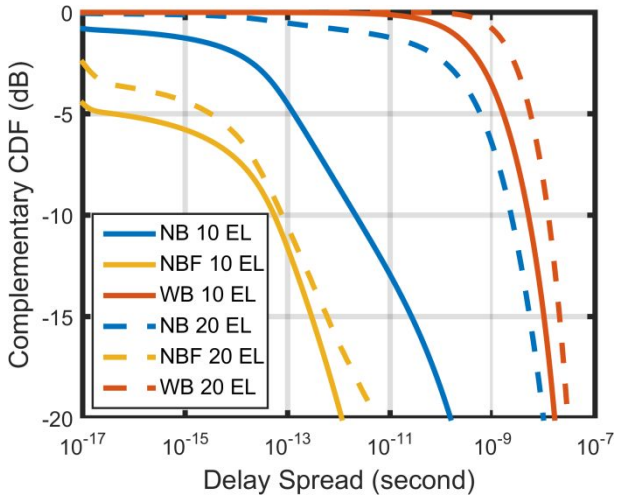

Figure 8: Delay spread of transmitted light in turbid harbor water for the narrow beam (NB), 10 mrad filtered narrow beam (NBF) and wide beam (WB).

6. ENERGY TRANSFER

We next look at the total energy transfer efficiency as a function of the receiver's aperture radius. We start with an aperture radius that is the narrow-beam beam waist (0.5 cm), and increase it to 10 times the beam waist (5 cm). We again look at both water types and transmitters, and include the 10 mrad filtering for the narrow beam. These plots are presented in Figure 9 and Figure 10.

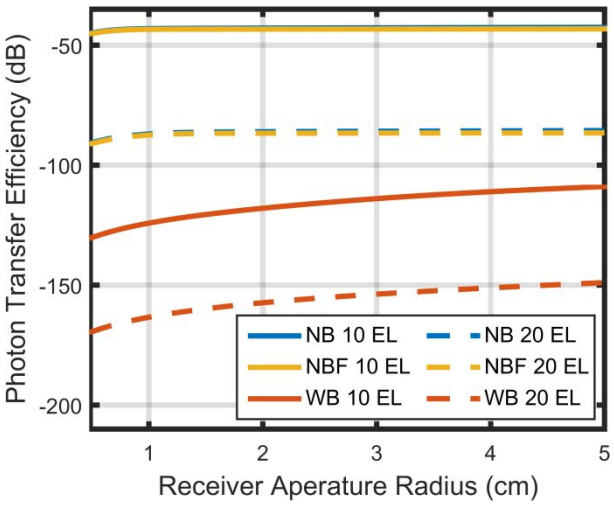

Figure 9: Energy transfer in clear ocean water for receiver aperture radius between $r = w_0$ (0.5 cm) and $r = 10\ w_0$ (5 cm). The narrow beam (NB) transfer efficiency drops by only 1-2 dB when a 10 mrad AoA filter is applied (NBF), and the plots overlap (blue and gold).

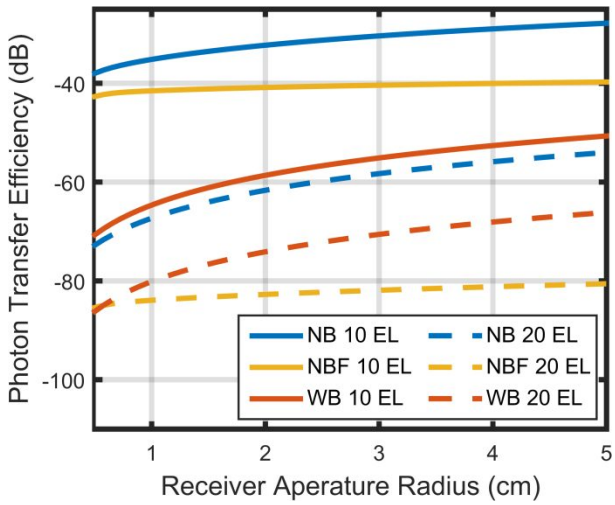

Figure 10: Energy transfer in turbid harbor water for receiver aperture radius between $r = w_0$ (0.5 cm) and $r = 10\ w_0$ (5 cm). The narrow beam (NB) transfer efficiency drops by 5-10 dB at 10 EL and 10-20 dB at 20 EL when a 10 mrad AoA filter is applied (NBF). The difference grows with aperture radius.

We find that in the clear ocean, increasing the receiver radius has little effect on the narrow beam energy transfer efficiency once the aperture radius is larger than twice the beam waist (1 cm). The AoA filtering does not significantly impact the energy transfer, with ~85% efficiency at 10 EL, and ~80% efficiency at 20 EL relative to the unfiltered beam. Qualitatively similar behavior with regards to AoA filtering of the narrow beam in the clear ocean is seen for the delay spread in Figure 7, and both are because most of the arriving light is unscattered. For the wide beam, however, increasing the detector radius continually increases the received number of photons, with about 20 dB improvement from $r = w_0$ to $r = 10w_0$ in the energy transfer efficiency. However, its total efficiency is still ~70 dB lower than the narrow beam at $r = 10w_0$.

In the harbor, where the scattering albedo is higher and the propagation distances shorter, filtering has a stronger effect. The unfiltered narrow-beam and wide-beam efficiencies grow at similar rates with increasing aperture radius, with the narrow beam efficiency being ~10dB higher at 10 EL and ~15 dB higher at 20 EL. Filtering the narrow beam greatly reduces its energy transfer efficiency, especially at 20 EL, and increasing the receiver aperture radius is no longer helpful; this is because the light outside the main lobe is mostly scattered light with a wide angular spectrum and is filtered out. As a result, at 20 EL the wide beam has the same energy transfer efficiency as the filtered narrow beam at $r = w_0$, and is over 10 dB greater at $r = 10w_0$. In this we see a tradeoff for narrow beams in turbid harbor water; AoA filtering will reduce ISI but also reduce the total energy transfer efficiency. The combined effect on communication data rates is unclear, so we now analyze the information capacity of the undersea channel for these system concepts.

7. ACHIEVABLE COMMUNICATION PERFORMANCE PREDICTIONS

The purpose of our propagation modeling is to predict optical communication performance. In particular, we use the simulation results to compare achievable performances with wide-beam and narrow-beam underwater communication systems. To do so, we assert several practical system constraints and then use information theory to compute the channel capacity given those constraints. Modern forward error correction (FEC) codes, such as low density parity check (LDPC) and turbo codes, have demonstrated performance approaching capacity limits[17]; as such the constrained capacity provides a readily computable stand-in for the achievable performance. We assume a $P_{Tx} = 0.1$ Watt peak power signal, with the narrow-beam a Gaussian shape with radial waist of 0.5 cm and the wide beam a point source uniformly distributed over the hemisphere. We will assume a non-return-to-zero (NRZ), on-off keyed (OOK) transmit waveform with perfect extinction (i.e. no photons are transmitted for a 0 symbol). The direct-detection receiver is characterized by

Poisson statistics (i.e. ideal photon counting). First, we calculate the received signal strength $N_S = P_{Tx}T_S L_{ch} h\nu$, where T_S is the symbol period, L_{ch} is the fraction of photons that arrive from the transmitter (determined by the propagation simulation), and $h\nu$ is the photon energy in joules. We also calculate the "noise" light level $N_B = N_{solar} + N_{ISI}$ due to the solar background light and scattered signal light. The propagation simulation provides the fraction L_{ISI} of transmit photons delayed by channel multi-path to cause inter-symbol interference; we calculate $N_{ISI} = P_{Tx}T_S L_{ISI} h\nu$. N_S and N_B have units of photons per symbol period.

To calculate the constrained channel capacity, we calculate $N_1 = N_S + N_B$ and $N_0 = N_B$, the average number of photons detected when a 1 or 0 is transmitted, respectively. The channel input is defined as $X \in \{0,1\}$, with equally likely inputs. The channel output Y is Poisson distributed given the input: $p_{Y|X}(y|x) = \frac{N_x^y e^{-N_x}}{y!}$. The mutual information $I(X;Y)$ is a straightforward computation and represents the channel capacity given the assumed constraints and channel model;since modern FEC codes can operate within 1 dB of capacity, this is a reasonable metric for achievable performance

Before turning to performance predictions, we note that the solar background light levels can significantly impact the channel capacity. Such levels vary widely depending on such factors as time of day, water clarity, terminal depth, link orientation (vertical or horizontal), wavelength, etc. In addition, terminal design choices such as angular and spectral filtering greatly affect the fraction of solar background coupled to the receiver. Indeed, a benefit of tracked, narrow-beam lasercom is the ability to filter out background light through restricted fields of view and the narrow spectral filtering thus enabled. We will examine cases with a high background, referenced to the "Gulf Stream" data[18]; the hemispherical down-welling irradiance values are 62.2 μW/cm^2/nm for 469 nm (used in the clear ocean case) and 79.2 μW/cm^2/nm for 518 nm (used in the harbor). We will also examine scenarios with no background light, corresponding to deep water and/or night time operations; in these cases stray light is due entirely to inter-symbol interference.

We begin with the turbid harbor cases. In Figure 11, we see the achievable OOK performance for selected wide-beam and narrow-beam systems in a high background case. We compare narrow-beam systems of 2 cm and 10 cm receive aperture diameters to a wide-beam system with a 10 cm aperture. The narrow-beam systems are angularly filtered to AoA<100 mrad. For the highest data rate, we see that the narrow-beam systems both significantly outperform the wide-beam system in terms of achievable range. Such performance is due primarily to the scattering-induced ISI that occurs with high-rate signaling. For lower rates, we see that the wide-beam system with a 10 cm aperture can achieve slightly longer distances than the 2 cm narrow-beam receiver. The scattered light collected in the larger aperture outweighs the narrow-beam's directional gain. The energy transfer of a narrow-beam transmission and a 10 cm receiver achieves the best performance.

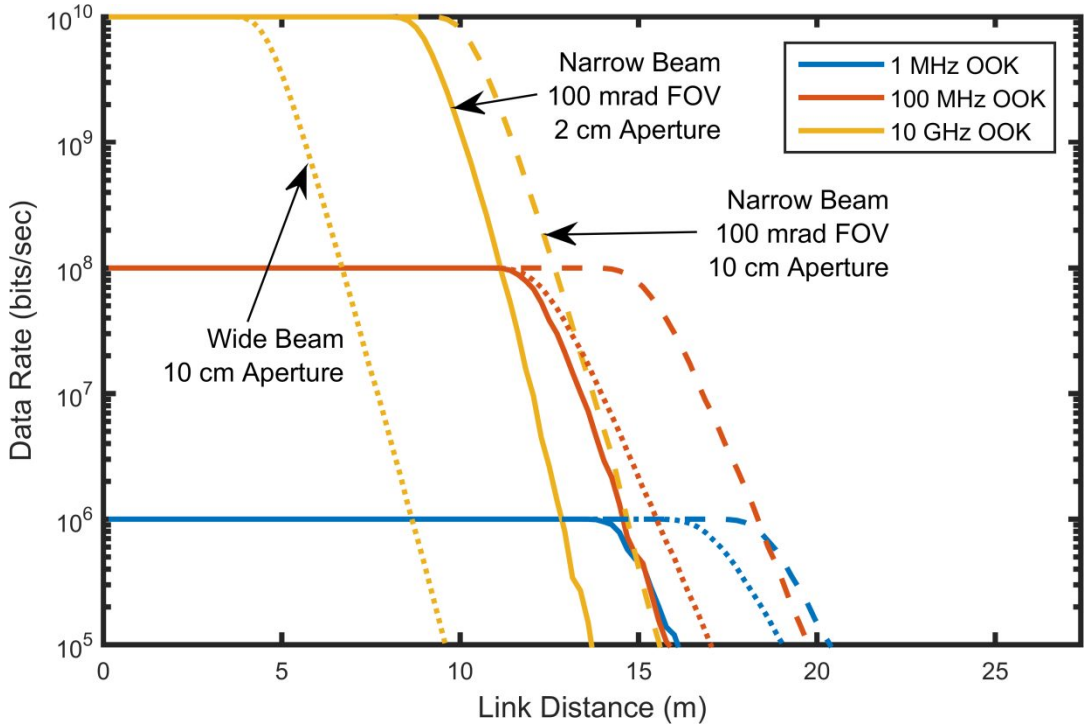

Figure 11 Turbid harbor comparison of narrow-beam and wide-beam systems in a high background light scenario. The different colors represent OOK clock rates of 10 GHz (yellow), 100 MHz (red), and 1 MHz (blue). The solid line represents the achievable performance of the narrow-beam system with a 100 mrad FOV and 2 cm receiver aperture, the dashed line a narrow-beam system with a 10 cm receive aperture, and the dotted line a wide-beam system with 10 cm aperture

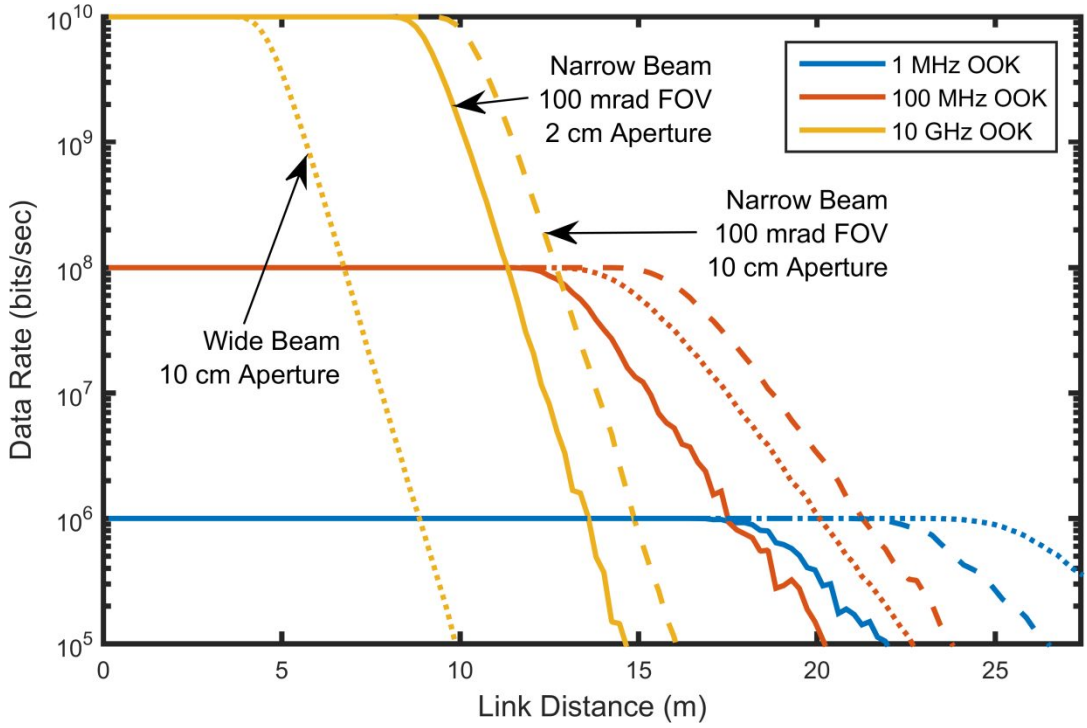

Figure 12 Turbid harbor comparison of narrow-beam and wide-beam systems with no background light. The colors and line markings match those of Figure 11.

The turbid harbor comparison with no background light is qualitatively similar to the high background scenario, though the achievable distances are slightly greater. As shown in Figure 12, both narrow-beam systems outperform the wide beam system for the highest signaling rate of 10 GHz. The wide-beam performance exceeds the small aperture narrow-beam system for the slowest signaling. It should be noted that the achievable distances in the harbor are relatively small due to the large extinctions. Achievable distances vary only by a few meters across the cases.

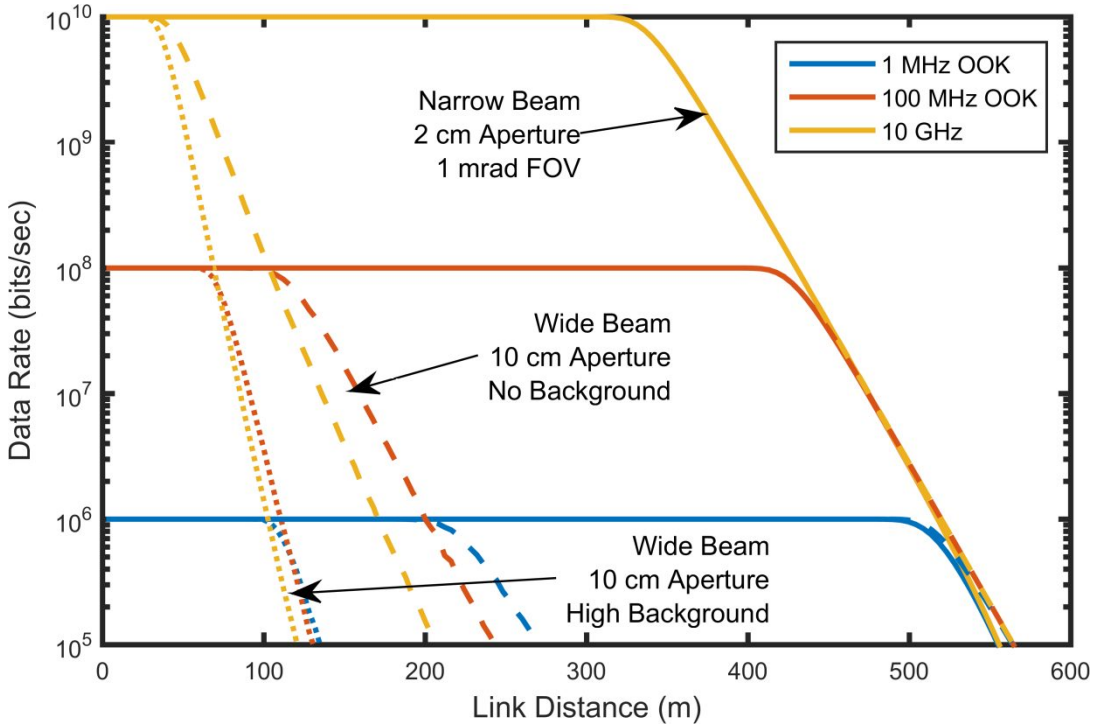

Figure 13 Clear ocean comparison of wide and narrow beam systems. The solid line represents the achievable performance of the narrow beam system with a 1 mrad FOV. (Data shown is for high background, however the no background performance is indistinguishable.) The wide beam performance is shown in dashed lines for the no background case and dotted lines for the high background case. The different colors represent OOK clock rates of 10 GHz (yellow), 100 MHz (red), and 1 MHz (blue).

We now turn our attention to the clear ocean cases, where we compare the achievable performance of the wide-beam and narrow-beam systems. We select the system components most favorable to each. The narrow-beam system utilizes a 2 cm receive aperture diameter and a 1 mrad field of view angular filter. The wide-beam system has a 10 cm receive aperture and a hemispherical field of view. We computed the performance achieved with OOK clock rates of 10 GHz, 100 MHz, and 1 MHz. The comparison is shown in Figure 13. For any given data rate, the narrow-beam system can achieve significantly longer distances than can the wide-beam system. This is particularly true for the higher data rates. We also see that the wide-beam system is more constrained by background light, while the performance of the narrow-beam system with a narrow FOV filter is virtually indistinguishable for the two background light cases. For the narrow-beam system in the clear ocean water, we predict performances of greater than 1 Gbps out to distances of 400 meters. We also note that the wide-beam predicted performance with no background is comparable with reported demonstrations[1].

We explore the aperture size and field of view selection in more detail in Figure 14. For the clear ocean with high background, we see that the narrow beam field of view filtering significantly affects the achievable range by reducing the background light levels. On the other hand, increasing the receive aperture size has almost no effect; most of the signal light that arrives at the receiver is still contained in the collimated beam of 1 cm diameter. For the wide beam,

however, a larger receive aperture provides significant benefit in the achievable range. These are the same trends seen in Figure 9 for the energy transfer efficiencies in clear ocean water.

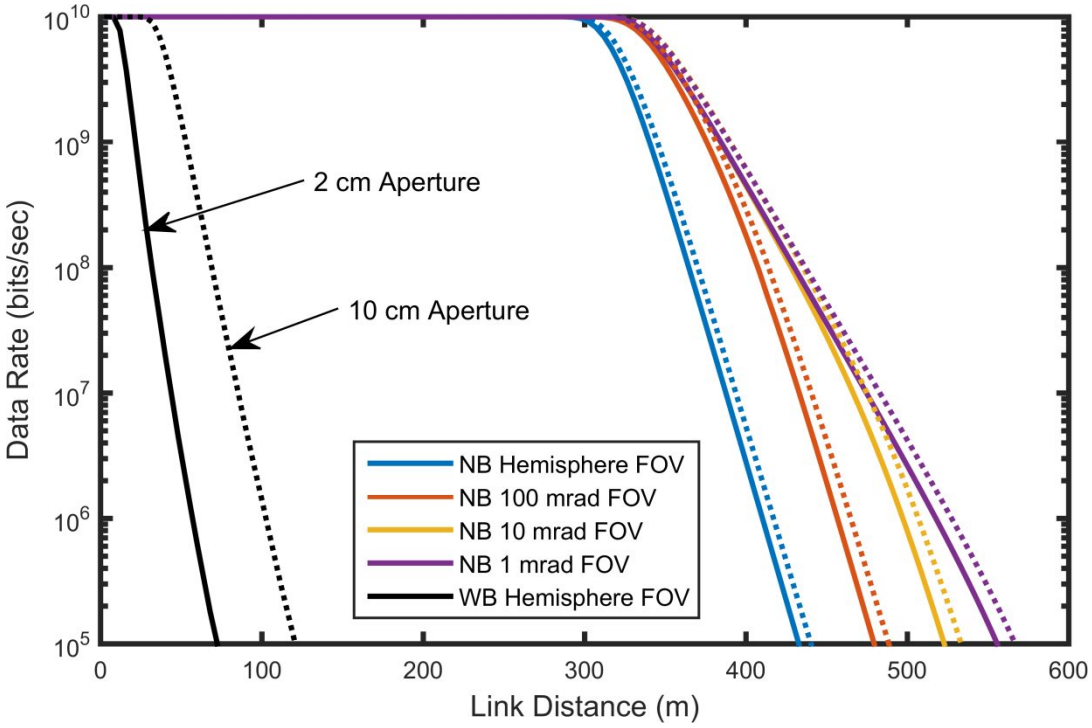

Figure 14 Aperture and field of view comparison for the clear ocean, high background case. 10 cm receive aperture is illustrated with dashed lines; 2 cm receive aperture with solid lines.

8. CONCLUSION

Propagation modeling shows significant performance advantages for narrow-beam undersea lasercom, compared to wide-beam optical communication. For the same data rate, the narrow beam system can achieve longer link distances, particularly for clear ocean waters. By engineering a precise pointing system, a narrow angular filter reduces the impact of background light and inter-symbol interference, enabling a higher data rate. Through the propagation modeling, we can systematically study lasercom system design trades and quantify the benefit of solving narrow-beam pointing, acquisition, and tracking.

REFERENCES

[1] C. Pontbriand, N. Farr, J. Ware, J. Preisig and H. Popenoe, "Diffuse high-bandwidth optical communications," in *OCEANS*, 2008.

[2] N. Farr, A. Bowen, J. Ware, C. Pontbriand and M. Tivey, "An integrated, underwater optical /acoustic communications system," in *OCEANS 2010 IEEE*, Sydney, 2010.

[3] N. Farr, J. Ware, C. Pontbriand, T. Hammar and M. Tivey, "Optical communication system expands CORK seafloor observatory's bandwidth," in *OCEANS 2010*, 2010.

[4] K. Nakamura, I. Mizukoshi, and M. Hanawa, "Optical wireless transmission of 405 nm, 1.45 Gbit/s optical IM/DD-OFDM signals through a 4.8 m underwater channel," *Opt. Express,* vol. 23, pp. 1558-1566, 2015.

[5] F. Hanson and S. Radic, "High bandwidth underwater optical communication," *Applied Optics,* Vols. 47, 2008, pp. 277-283.

[6] H. M. Oubei, C. Li, K. Park, T. K. Ng, M. Alouini, and B.S. Ooi, "2.3 Gbit/s underwater wireless optical communications using directly modulated 520 nm laser diode," *Optics Express,* vol. 23, no. 16, pp. 20743-20748, 2015.

[7] H. M. Oubei, J. R. Duran, B. Janjua, H. Wang, C. Tsai, Y. Chi, T. K. Ng, H. Kuo, H. He, M. Alouini, G. Lin, and B. S. Ooi, "4.8 Gbit/s 16-QAM-OFDM transmission based on compact 450-nm laser for underwater wireless optical communication," *Opt. Express,* vol. 23, pp. 23302-23309, 2015.

[8] D. M. Boroson, B. S. Robinson, D. V. Murphy, D. A. Burianek, F. Khatri, J. M. Kovalik, Z. Sodnik and D. M. Cornwell, "Overview and Results of the Lunar Laser Communication Demonstration," *Proc. SPIE,* Vols. 8971, 2014, pp. 89710S-1 - 89710S-11.

[9] C. D. Mobley, B. Gentili, H. R. Gordon, Z. Jin, G. W. Kattawar, A. Morel, P. Reinersman, K. Stamnes and R. H. Stavn, "Comparison of Numerical Models for Computing Underwater Light Fields," *Applied Optics,* 1993.

[10] C. Gabriel, M.-A. Khalighi, S. Bourennane, P. Leo and V. Rigaud, "Monte-Carlo-Based Channel Characterization for Underwater Optical Communication Systems," *Journal of Optical Communications and Networking,* vol. 5, no. 1, 2013.

[11] J. W. McLean, J. D. Freeman and R. E. Walker, "Beam Spread Function with Time Dispersion," *Applied Optics,* vol. 37, no. 21, 1998.

[12] Y. Dong, H. Zhang and X. Zhang, "On Impulse Response Modeling for Underwater Wireless Optical MIMO links," Communications in China (ICCC), 2014 IEEE/CIC International Conference on, 2014.

[13] V. Jagadeesh, A. Choudhary, F. M. Bui and P. Muthuchidambaranathan, "Characterization of Channel Impulse Responses for NLOS Underwater Wireless Optical Communications," in *Fourth International Conference on Advances in Computing and Communications*, 2014.

[14] C. D. Mobley, Light and Water, Academic Press, 1994.

[15] T. J. Petzold, "Volume Scattering Functions for Selected Ocean Waters," Scripps Institution of Oceanography, La Jolla, CA, 1972.

[16] N. Jerlov, Marine Optics, Amsterdam: Elsevier Scientific Pub Co., 1976.

[17] T. Richardson and R. Urbanke, Modern Coding Theory, New York, NY: Cambridge University Press, 2008.

[18] J. E. Tyler and R. C. Smith, Measurement of Spectral Irradiance Underwater, New York, NY: Gordon & Breach, 1970.